Phase dynamics in intrinsic Josephson junctions and their electrodynamics

Shizeng Lin[1,2] and Xiao Hu[1,2,3]
[1]*WPI Center for Materials Nanoarchitectonics, National Institute for Materials Science, Tsukuba 305-0044, Japan*
[2]*Graduate School of Pure and Applied Sciences, University of Tsukuba, Tsukuba 305-8571, Japan*
[3]*Japan Science and Technology Agency, 4-1-8 Honcho, Kawaguchi, Saitama 332-0012, Japan*
(Received 30 September 2008; revised manuscript received 20 January 2009; published 11 March 2009)

We present a theoretical description of the phase dynamics and its corresponding electrodynamics in a stack of inductively coupled intrinsic Josephson junctions of layered high-T_c superconductors in the absence of an external magnetic field. Depending on the spatial structure of the gauge-invariant phase difference, the dynamic state is classified into: state with kink, state without kink, and state with solitons. It is revealed that in the state with phase kink, the plasma is coupled to the cavity and the plasma oscillation is enhanced. In contrast, in the state without kink, the plasma oscillation is weak. It points a way to enhance the radiation of electromagnetic from high-T_c superconductors. We also perform numerical simulations to check the theory and good agreement is achieved. The radiation pattern of the state with and without kink is calculated, which may serve as a fingerprint of the dynamic state realized by the system. At last, the power radiation of the state with solitons is calculated by simulations. The possible state realized in the recent experiments is discussed in the viewpoint of the theoretical description. The state with kink is important for applications including terahertz generators and amplifiers.

DOI: 10.1103/PhysRevB.79.104507 PACS number(s): 74.50.+r, 74.25.Gz, 85.25.Cp

I. INTRODUCTION

The electromagnetic waves in the terahertz region, which is defined in the range from 0.1 to 10 THz, have wide applications, such as drug detection, materials characterization, security check, and so on. This has sparked considerable efforts to seek compact and low-cost solid-state generators.[1,2]

It has been known for a long time that Josephson junctions can be used as electromagnetic oscillators. The power radiated from a single junction, however is in the range of picowatts, which is too small for practical applications. The frequency is about one hundred gigahertz because of the small superconducting energy gap for conventional superconductors.[3–6] Although one may integrate a large array of Josephson junctions made of conventional superconductors on a chip to enhance the radiation power,[7–10] the frequency is still below terahertz. The discovery of intrinsic Josephson junctions in layered high-T_c superconductors, such as $Bi_2Sr_2CaCu_2O_{8+\delta}$ (BSCCO) provides a very nice candidate for terahertz oscillator.[11] The advantages of intrinsic Josephson junctions over conventional low-temperature junctions are as follows. First, the junctions are homogeneous in the atomic scale, which makes the coherent radiation in large number of junctions possible. Second, the energy gap is about 60 meV which corresponds to 15 THz. The terahertz Josephson plasma if excited is thus free from Landau damping.[12]

One idea to excite the terahertz wave inside the intrinsic Josephson junctions is by the motion of Josephson vortices lattice induced by an in-plane magnetic field and a transport current, which has already been investigated both theoretically and experimentally.[13–19] In spite of these works, it is still lack of clear evidence of coherent radiation. Radiation from BSCCO with injection of quasiparticles has been reported.[20–24] Alternatively, the terahertz radiation without a magnetic field has also been attempted.[25–29] Recently, a strong coherent radiation from BSCCO in the absence of a magnetic field was observed,[27,29] where the mesa of the single crystal of BSCCO forms a cavity. The breakthrough in the experiments has inspired considerable theoretical and experimental efforts, aiming to reveal the mechanism of strong radiation.[30–35] A new dynamic state has been suggested to explain the experiments.[30,31]

It is well known that there exist various dynamic states, such as the McCumber state and states with solitons, with different *IV* characteristics in a Josephson junction[30,36] due to the nonlinearity. In the McCumber state, the gauge-invariant phase difference is uniform in space, which we will refer to as the state without kink in later discussions. The soliton solutions are also well known, especially in a single junction, where a quantized particlelike object of 2π phase variation travels along the junction. Recently, a new dynamic state was found, where a $(2m+1)\pi$ phase kink is localized inside the junction with an integer m.[30,31] We will refer to this state hereafter as state with kink. Because of the complexity in the dynamics in this highly nonlinear system, theoretical understanding of phase dynamics and its electrodynamics, and finding the optimal state are expected to be helpful for experimental realizations of terahertz generators. Assessments of such a device from a theoretical aspect are also needed.

For this purpose, in this paper we provide more details on the new dynamic state found in the previous study.[30] In Sec. II, we first derive the Lagrangian of a stack of Josephson junctions based on the superconductor-insulator-superconductor (SIS) model. From the Lagrangian we derive the inductively coupled sine-Gordon equation. It also gives the power balance condition. In Sec. III, we develop a general procedure to solve the coupled sine-Gordon equation from the spectrum analysis, from which we derive the solutions with and without phase kink. We calculate analytically the *IV* characteristics and power radiation of the state with and without kink when the plasma oscillation is small. Numerical simulations are performed to verify the analytical solutions

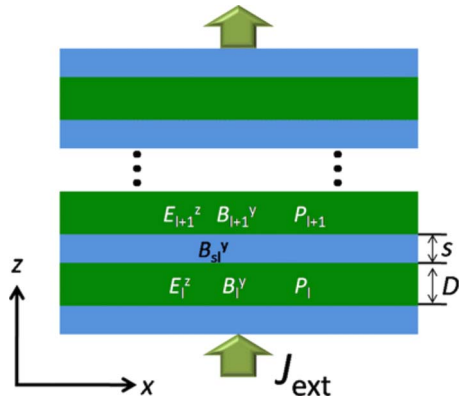

FIG. 1. (Color online) Schematic view of a stack of Josephson junctions based on the SIS model. The blue/light (green/dark) area denotes superconducting (insulating) layers.

and good agreement is attained. In Sec. IV, the energy stored in the system is evaluated. In Sec. V, the far-field radiation pattern from the mesa is calculated both at state with and without kink, which can be used to distinguish the different dynamic states. In Sec. VI, the power radiation from the state with solitons is investigated by simulations for comparison. At last, the paper is concluded with a short discussion.

II. LAGRANGIAN AND MODEL EQUATION

The geometry we consider is depicted in Fig. 1. We neglect the thermal fluctuations so that the amplitude $|\Delta|$ of the superconducting order parameter $|\Delta|\exp(i\psi)$ is constant. Furthermore, ψ along the y axis is assumed to be uniform, namely, we concentrate on the zero mode along this direction. The system is then reduced to two dimensions. The density of energy stored in the superconducting layers, which consists of supercurrent energy and magnetic energy, then can be written as

$$H_{\rm sl}(x) = \frac{1}{8\pi}\int_{l(s+D)+D}^{(l+1)(s+D)} [\lambda_s^2(\nabla \times B_{\rm sl}^y)_x^2 + B_{\rm sl}^{y2}]dz, \qquad (1)$$

where λ_s is the penetration depth, and $B_{\rm sl}^y$ is the magnetic field in the lth superconducting layer. The energy stored in the insulating layers is the sum of energy of electromagnetic wave and Josephson energy

$$H_{\rm bl}(x) = \int_{l(s+D)}^{l(s+D)+D} \left(\frac{B_l^{y2}}{8\pi} + \frac{\epsilon_c E_l^{z2}}{8\pi}\right)dz + \frac{\Phi_0}{2\pi c}J_c(1-\cos P_l), \qquad (2)$$

where B_l^y (E_l^z) is the magnetic (electric) field in the lth insulating layer (their variation along the z direction in the lth insulating layer will be neglected in later treatment). J_c is the critical current density, ϵ_c dielectric constant along the z axis, and c the light velocity in vacuum. P_l is the gauge-invariant phase difference defined as

$$P_l(x) = \psi_{l+1}(x) - \psi_l(x) - \frac{2\pi}{\Phi_0}\int_{l(s+D)}^{l(s+D)+D} A_l^z(x)dz, \qquad (3)$$

where $\Phi_0 \equiv hc/2e$ is the flux quantum and A_l^z is the vector potential. The magnetic field inside the superconducting layer can be evaluated from the London equation $B_{\rm sl}^y(z) = (\sinh[(s-z)/\lambda_s]B_l^y + \sinh[z/\lambda_s]B_{l+1}^y)/\sinh[s/\lambda_s]$. In high-$T_c$ superconductors, the thickness of superconducting layer s and insulating layer D is much smaller than λ_s, we have $B_{\rm sl}^y \simeq [(s-z)B_l^y + zB_{l+1}^y]/s$. Then the total-energy density can be expressed as

$$\begin{aligned} H(x) &= \sum_l [H_{\rm sl}(x) + H_{\rm bl}(x)] \\ &= \sum_l \left\{ \frac{D}{8\pi}[(2\zeta+1)B_l^{y2} - \zeta(B_{l+1}^y B_l^y + B_l^y B_{l-1}^y)] \right. \\ &\quad \left. + D\frac{\epsilon_c E_l^{z2}}{8\pi} + \frac{\Phi_0}{2\pi c}J_c(1-\cos P_l)\right\}, \end{aligned} \qquad (4)$$

where we have neglected the surface effect along the stack direction, which is valid for thick stacks of junctions. $\zeta \equiv \lambda_s^2/sD$ is the strength of inductive coupling. It should be noted that the inductive coupling is very strong in BSCCO; see Table I.

To find the relation between the magnetic field B_l^y and P_l, we derive both sides of Eq. (3) with respect to x. With the London equation and Maxwell equation, we arrive at

$$\frac{\Phi_0}{2\pi D}\partial_x \mathbf{P} = \mathbf{M}\mathbf{B}^y, \qquad (5)$$

where $\mathbf{P}$ is a column vector $\mathbf{P}^T = [P_1, P_2, \ldots, P_N]$ with N being the number of junctions. The column vectors for other

TABLE I. Conversion of quantities among dimensionless, Gaussian, and SI units. Here λ_c and λ_{ab} are the penetration depth; ϵ_c is dielectric constant along the z axis; c is the light velocity in vacuum; ϵ_0 is dielectric constant in vacuum; $\omega_p = c/\lambda_c\sqrt{\epsilon_c}$ is the Josephson plasma frequency. $J_c = c\Phi_0/8\pi^2\lambda_c^2 D$ is the critical current density. In the present paper, we use $\lambda_c = 200$ μm, $\lambda_{ab} = 0.4$ μm, $\epsilon_c = 10$, $s = 0.3$ nm, and $D = 1.2$ nm, which are typical for BSCCO. Then $\lambda_s = \sqrt{sD/(s+D)^2}\lambda_{ab} = 0.16$ μm. The two dimensionless parameters are then $\beta = 0.02$ and $\zeta = 7.1\times 10^4$. Following Ref. 30, we use slightly larger $\zeta = 4/9\times 10^6$ in the present paper, and the results are insensitive to ζ as far as it is large. The length of junction is $L = 80$ μm.

	Length	Time	Conductance	Electric field	Voltage	Magnetic field	Poynting vector	Current	Impedance
Dimensionless	x	t	β	E	V	B	S	J	Z
Gaussian	$\lambda_c x$	t/ω_p	$c\sqrt{\epsilon_c}\beta/4\pi\lambda_c$	$\Phi_0\omega_p E/2\pi cD$	$\Phi_0\omega_p V/2\pi c$	$\Phi_0 B/2\pi\lambda_c D$	$\Phi_0^2\omega_p EB/16\pi^3 D^2\lambda_c$	$\frac{Jc\Phi_0}{8\pi^2\lambda_c^2 D}$	$Z/\sqrt{\epsilon_c}$
SI	$\lambda_c x$	t/ω_p	$c\sqrt{\epsilon_c\epsilon_0}\beta/\lambda_c$	$\Phi_0\omega_p E/2\pi D$	$\Phi_0\omega_p V/2\pi$	$\Phi_0 B/2\pi\lambda_c D$	$\Phi_0^2\omega_p EB/4\pi^2\mu_0 D^2\lambda_c$	$\frac{J\Phi_0}{2\pi\lambda_c^2 D\mu_0}$	$Z/\sqrt{4\pi\epsilon_c\epsilon_0}$

quantities are defined in the same way. $\mathbf{M}$ is the inductive coupling matrix defined as[37,38]

$$\mathbf{M} = \begin{bmatrix} 2\zeta+1 & -\zeta & 0 & \cdots & & 0 & -\zeta \\ -\zeta & 2\zeta+1 & -\zeta & 0 & \cdots & & 0 \\ 0 & \ddots & \ddots & \ddots & 0 & \cdots & \\ \cdots & 0 & -\zeta & 2\zeta+1 & -\zeta & 0 & \cdots \\ & \cdots & 0 & \ddots & \ddots & \ddots & 0 \\ 0 & & \cdots & 0 & -\zeta & 2\zeta+1 & -\zeta \\ -\zeta & 0 & & \cdots & 0 & -\zeta & 2\zeta+1 \end{bmatrix}, \tag{6}$$

where the periodic boundary condition along the z axis is imposed. Using the ac Josephson relation $\partial_t \mathbf{P} = 2e\mathbf{E}^z D/\hbar$ and Eq. (5), we can rewrite the total-energy density in a compact form,

$$H(x) = \frac{1}{2}\partial_x \mathbf{P}^T \mathbf{M}^{-1} \partial_x \mathbf{P} + \frac{1}{2}\partial_t \mathbf{P}^T \partial_t \mathbf{P} + \sum_l (1 - \cos P_l), \tag{7}$$

where the dimensionless quantities have been used, which, with the conversion among SI units and Gaussian units, are compiled in Table I. The first term at the right-hand side of Eq. (7) represents the magnetic energy, the second term the electric energy, and the last term the Josephson coupling. The Lagrangian corresponding to Eq. (7) is

$$\mathcal{L}(x) = \frac{1}{2}\partial_x \mathbf{P}^T \mathbf{M}^{-1} \partial_x \mathbf{P} + \frac{1}{2}\partial_t \mathbf{P}^T \partial_t \mathbf{P} - \sum_l (1 - \cos P_l). \tag{8}$$

With the Euler-Lagrangian formula, we arrive at the coupled sine-Gordon equation

$$\partial_x^2 \mathbf{P} = \mathbf{M}[\sin \mathbf{P} + \partial_t^2 \mathbf{P}], \tag{9}$$

where $\sin \mathbf{P} \equiv [\sin P_1, \sin P_2, \ldots, \sin P_N]^T$. We consider the overlap geometry[37] where the current is uniformly injected into the system. Taking the dissipation and external current into account, we obtain the inductively coupled perturbed sine-Gordon equation,

$$\partial_x^2 \mathbf{P} = \mathbf{M}[\sin \mathbf{P} + \partial_t^2 \mathbf{P} + \beta \partial_t \mathbf{P} - \mathbf{J}_{\text{ext}}], \tag{10}$$

where the first term on the right-hand side of Eq. (10) is the Josephson current, the second term is the displacement current, the third term is the quasiparticles contribution and the last term the external current. Writing down the equation for P_l in Eq. (10) explicitly, we have

$$\partial_x^2 P_l = (1 - \zeta \Delta^{(2)})[\sin P_l + \partial_t^2 P_l + \beta \partial_t P_l - J_{\text{ext}}], \tag{11}$$

where $\Delta^{(2)}$ is the finite difference operator defined as $\Delta^{(2)} f_l \equiv f_{l+1} + f_{l-1} - 2f_l$. Besides the inductive coupling in Eq. (10), a capacitive coupling[39,40] and a coupling originating from nonequilibrium effects[41,42] are also present in intrinsic Josephson junctions. These two couplings are weak in comparison to the inductive coupling and are neglected in the present work.

The above calculations are based on the SIS model (superconductor-insulator-superconductor), which is a good model for artificially stacked Josephson junctions. However, for BSCCO, the superconducting layer is only of atomic thickness, and thus the quantity λ_s is not well defined. To find the relation between λ_s and the measurable penetration depth λ_{ab}, we need to resort to the Lawrence-Doniach model, which has already been discussed extensively in literatures. The connection between λ_s and λ_{ab} is given by $\lambda_s = \sqrt{sD/(s+D)^2}\lambda_{ab}$.[43,44]

In the presence of dissipations and a power input, the energy oscillates with time according to

$$\partial_t H(x) = \partial_{xt} \mathbf{P}^T \mathbf{M}^{-1} \partial_x \mathbf{P} + (\partial_t^2 \mathbf{P}^T + \sin \mathbf{P}^T) \partial_t \mathbf{P}. \tag{12}$$

With the help of Eq. (10), we have for the steady state

$$\int_0^T \int_0^L \partial_t H dx dt = \int_0^T (\partial_t \mathbf{P}^T \mathbf{M}^{-1} \partial_x \mathbf{P})|_0^L dt + \int_0^T \int_0^L \partial_t \mathbf{P}^T \mathbf{J}_{\text{ext}} dx dt - \beta \int_0^T \int_0^L \partial_t \mathbf{P}^T \partial_t \mathbf{P} dx dt = 0, \tag{13}$$

where L is the length of junctions and T is the period of plasma oscillation. Rewriting Eq. (13) in a more transparent form, we have the power balance condition,

$$\int_0^T (\mathbf{E}^T \mathbf{B})|_0^L dt + LT \mathbf{E}_{\text{dc}}^T \mathbf{J}_{\text{ext}} - \beta \int_0^T \int_0^L \mathbf{E}^T \mathbf{E} dx dt = 0, \tag{14}$$

where the first term is the power gain (loss) at edges due to irradiation (radiation). The second term is the input power with $\mathbf{E}_{\text{dc}}$ the dc electric field, and the last term is the energy loss due to dissipations. It should be remarked that Eq. (14) is general and should be valid at different states. As will be shown later, the power balance relation is useful when the plasma oscillation is strong and the linear expansion fails. From Eq. (14) and $\mathbf{E} = \mathbf{E}_{\text{ac}} + \mathbf{E}_{\text{dc}}$, we can see that when the oscillation in electric field $\mathbf{E}_{\text{ac}}$ is small, the *IV* curve is almost Ohmic $\mathbf{E}_{\text{dc}} \approx \mathbf{J}_{\text{ext}}/\beta$. To have strong radiation, the oscillation of electric field in the junctions should be large. Therefore the optimal state for the radiation is a state having nonlinear *IV* characteristics where a large part of the input power can be pumped into plasma oscillation. The problem then boils down to finding such a state with highly nonlinear *IV* characteristics.

The relation between the oscillating magnetic field and electric field at the edges of junctions is given by the boundary condition. The boundary condition depends on many effects such as distribution of the order parameter near edges, the geometry of the sample, and the dielectric materials attached to the sample. In Refs. 16 and 45, the dynamic boundary condition is derived from the electromagnetic wave equations inside the dielectrics. In the present paper, we use an effective impedance as the boundary condition,

$$\mathbf{E}_{\text{ac}}/\mathbf{B}_{\text{ac}} = Z = |Z(\omega)| \exp[i\theta(\omega)], \tag{15}$$

where $|Z|$ and θ are parameters, and ω is the frequency. This boundary condition is general and any other boundary con-

dition can be cast into this form. It has been pointed out that there is a significant impedance mismatch between the intrinsic Josephson junctions and outside space because of the small ratio between the thickness of the stack and the penetration depth λ_c.[28] This means $|Z| \gg 1$, which is similar to the single junction case.[46]

The radiation power counted by Poynting vector at one edge with an effective impedance becomes

$$S_r = \frac{1}{2TN}\int_0^T \mathrm{Re}[\mathbf{E}_{\mathrm{ac}}^{\dagger}\mathbf{B}_{\mathrm{ac}}]dt = \frac{\cos\theta}{2T|Z|N}\int_0^T \mathbf{E}_{\mathrm{ac}}^{\dagger}\mathbf{E}_{\mathrm{ac}}dt. \quad (16)$$

For ease of theoretical calculation, we consider the situation that the radiation does not substantially change the plasma oscillation inside the junctions. In this case, $\mathbf{E}_{\mathrm{ac}}$ can be evaluated *without* radiation, i.e., with the simple boundary condition $\partial_x \mathbf{P}=0$. This treatment is valid when the impedance mismatch is significant, which will be shown later to be rather accurate by numerical simulations. When the impedance $|Z|$ is small, however, one should take the effect of radiation into account in the calculation of the plasma dynamics self-consistently.

III. SOLUTIONS

In this section, we first construct a general procedure to solve the coupled sine-Gordon equation from the spectrum analysis. There exist longitudinal and transverse plasma modes in a stack of junctions. As the stack itself forms a cavity, the plasma component can be written as $\tilde{P}_l(x) \sim \cos(k_j x)\sin[ql/(N+1)]$ (Refs. 47 and 48) with $k_j = j\pi/L$, and q, j integers. There are N different dispersion branches with characteristic velocity $c_q = 1/\sqrt{1+2\zeta\{1-\cos[q\pi/(N+1)]\}}$. When the stack is thick enough, the plasma oscillation uniform along the c axis becomes possible and its velocity is $c_0=1$. We will concentrate on this case in the present work since it supports the strong radiation. Without an external in-plane magnetic field, the solution including all frequency harmonics subject to the boundary condition $\partial_x P_l=0$ can be expressed as[30]

$$P_l(x,t) = \omega t + P_l^s(x) + \sum_{j=1}^{\infty} \mathrm{Re}[-iA_j \exp(ij\omega t)]\cos(k_j x), \quad (17)$$

where ωt is the rotating part, P_l^s the static phase kink, and the last term is the plasma oscillation including all harmonics, with A_j the oscillation amplitude. For simplicity, the first cavity mode along the x axis with $k_1=\pi/L$ is considered and the small time dependence of P_l^s is neglected.[30,31] Putting the mth frequency component of the Josephson current $\sin P_l$ as $S_m^l \exp(im\omega t)$, and expanding sine of sine with Bessel functions, we have

$$S_m^l = G_m^l + G_{-m}^{l*}, \quad \text{for } m \geq 1,$$

$$S_0^l = G_0^l, \quad \text{for } m = 0, \quad (18)$$

where

$$G_m^l(x) = -i \sum_{\{q_j=-\infty\}}^{+\infty} \delta\left(\sum_{j=1}^{\infty} q_j j, m-1\right)\left\{\prod_{j=1}^{\infty} J_{q_j}[|A_j|\cos(k_j x)]\right\} \times \exp\left[i\left(P_l^s + \sum_{j=1}^{\infty} q_j \phi_j\right)\right], \quad (19)$$

with J_{q_j} the Bessel function of the first kind. $\Sigma_{\{q_j=-\infty\}}^{+\infty}$ is the summation over the ensemble of q_j's, and $A_j = |A_j|\exp(i\phi_j)$. Substituting Eq. (17) into the coupled sine-Gordon Eq. (11) and comparing each frequency component in $\sin P_l$, we have for the mth ($m \geq 1$) component,

$$[ik_m^2 - i(m\omega)^2 - \beta m\omega]A_m \cos(k_m x) = (1-\zeta\Delta^{(2)})S_m^l. \quad (20)$$

From Eq. (20), A_m is given by

$$A_m = \frac{F_m}{ik_m^2 - i(m\omega)^2 - m\beta\omega}, \quad (21)$$

with

$$F_m \equiv \frac{2}{L}\int_0^L (1-\zeta\Delta^{(2)})S_m^l \cos(k_m x)dx. \quad (22)$$

The functional F_m represents the coupling of the plasma to the cavity modes, which is the central quantity for the excitation of plasma. Other mechanism such as the modulation of the critical current is also possible,[28,49] although it is practically very hard to achieve a homogeneous modulation along the z axis. In the present solution, P_l^s is inherently one part of the solution. Since we have assumed that phase is uniform along the y direction, or equivalently, we have considered the (1,0) cavity mode, only the kink in the x direction contributes to F_m. If there exits a kink along the y direction simultaneously, the functional F_m will be enhanced further.[34] In the case of cylinder geometry, the plasma is coupled to the cavity fully via the kink so that F_m is maximized.[34]

It should be noted that A_m is independent of l in Eq. (21), which imposes a constraint on the arrangement of P_l^s in the z direction. As will be shown later, periodic arrangements such as those in Figs. 2(a) and 2(b) diagonalize the finite difference operator and make F_m independent of l.

For the 0th component (static part), we obtain

$$\partial_x^2 P_l^s - \beta\omega + J_{\mathrm{ext}} = (1-\zeta\Delta^{(2)})S_0^l. \quad (23)$$

The current conservation relation reads $J_{\mathrm{ext}} = \beta\omega + \langle S_0^l\rangle_x$ ($\langle\cdots\rangle_x$ is the spatial average). The remaining terms in Eq. (23) which do not contribute to the net current is

$$\partial_x^2 P_l^s = -\zeta\Delta^{(2)}S_0^l, \quad (24)$$

where $\zeta \gg 1$ is taken into account.

From Eqs. (17), (21), and (24), we can calculate the plasma oscillation, IV characteristics and P_l^s. We consider explicitly the case where the fundamental mode A_1 is small and thus higher harmonics can be safely neglected. We also approximate $J_1[|A_1|\cos(k_1 x)] \simeq |A_1|\cos(k_1 x)/2$ and $J_0[|A_1|\cos(k_1 x)] \simeq 1$. We will refer to this approximation as linear approximation in later discussions, and the validity of this approximation will become clear later. It should be noted

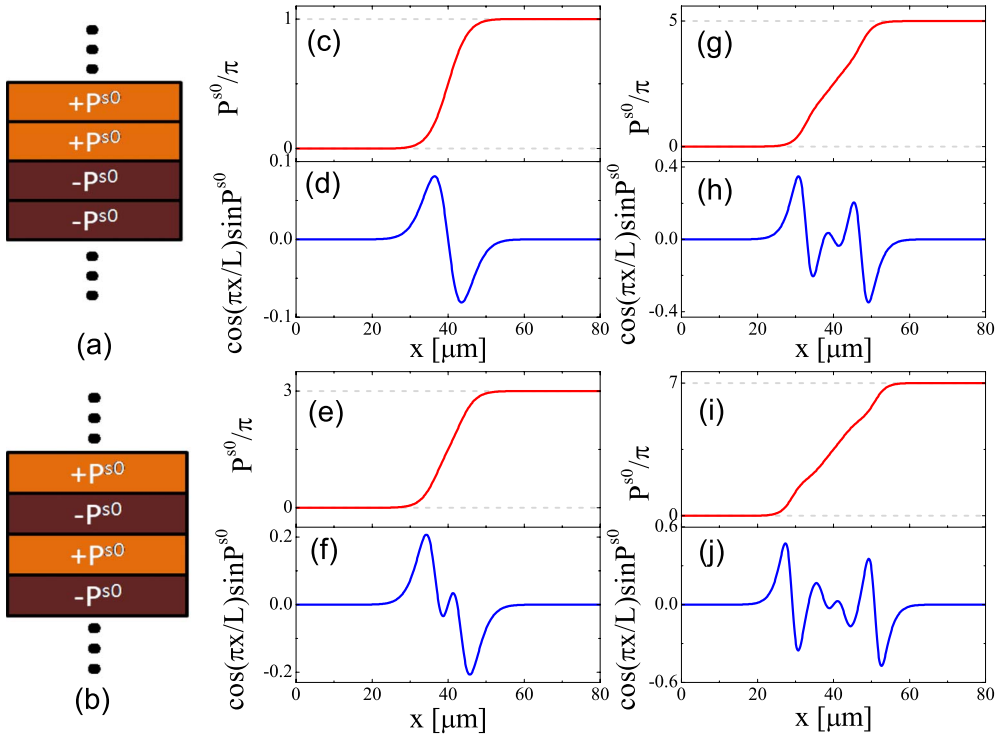

FIG. 2. (Color online) [(a) and (b)] Schematic view of two simplest configurations of the static phase $P_l^s(x)$. [(c), (e), (g) and (i)] $(2m+1)\pi$ phase kink for $m=0$, 1, 2, and 3, respectively. [(d), (f), (h), and (j)] Their corresponding unquantized static vortices.

that the nonlinearity of the coupled sine-Gordon equation is still retained in the equation for P_l^s, Eq. (24). With this approximation, we can calculate A_1

$$A_1 = \frac{F_1}{ik_1^2 - i\omega^2 - \beta\omega}, \tag{25}$$

where $F_1 = \frac{-2i}{L}\int_0^L (1-\zeta\Delta^{(2)})\exp(iP_l^s)\cos(k_1 x)dx$.

The IV characteristic is given by the current conservation

$$J_{\text{ext}} = \beta\omega + \langle S_0^l \rangle_x = \beta\omega + \frac{\beta\omega|F_1|^2/4}{(k_1^2-\omega^2)^2 + \beta^2\omega^2}, \tag{26}$$

where the first term at the right-hand side is the normal current and the second term is the dc part of the Josephson current.

The equation for P_l^s is given by

$$\partial_x^2 P_l^s = \frac{A_1\zeta i}{2}\cos(k_1 x)\Delta^{(2)}\exp(-iP_l^s). \tag{27}$$

Equation (27) has many solutions, such as the trivial vacua solution and solutions with phase kink, which will be discussed separately in Secs. III A and III B.

A. State with kink

Equation (27) has solutions with $(2m+1)\pi$ kink with m being an integer.[30,31] Let us consider the two simplest periodic configurations of P_l^s depicted in Figs. 2(a) and 2(b) where $P_l^s = f_l P^{s0}$ with $f_l = \pm 1$ depending on l, which diagonalize Eq. (27),

$$\partial_x^2 P^{s0} = \zeta q\ \text{Re}(A_1)\cos(k_1 x)\sin P^{s0}, \tag{28}$$

where $q=1$ for the configuration in Fig. 2(a) and $q=2$ for the configuration in Fig. 2(b). It should be noted that other periodic configurations are also possible. Equation (28) is invariant under the transformation $x \leftarrow L-x$ and $P^{s0} \leftarrow (2m+1)\pi - P^{s0}$, which clearly renders a kink at the center of junction. Equation (28) subject to the boundary condition $\partial_x P^{s0}=0$ is solved numerically and the results are detailed in the Fig. 2, where the $(2m+1)\pi$ phase kink of characteristic length $\lambda_P \equiv 1/\sqrt{\zeta q|\text{Re}(A_1)|}$ is at the center of junction $x=L/2$. It is this $(2m+1)\pi$ phase kink that pumps the dc power into plasma oscillation.

In Fig. 2, we can see that $\partial_x^2 P^{s0}$ forms an unquantized static vortex with characteristic length λ_P, therefore it does not contribute to the net supercurrent $\langle \sin P_l \rangle_{xt}$. There is a dc magnetic field in each layer associated with the static vortex. As it points in opposite directions in different junctions, the total magnetic field across the intrinsic Josephson junctions vanishes. Therefore it is impossible to realize the kink state in a single junction.

In addition to the $(2m+1)\pi$ phase kink, there exist the well-known solitons with 2π phase variation superposing to the $(2m+1)\pi$ phase kink, as observed in our simulations (not shown in Fig. 2). In the region of $|x_0 - L/2| \gg \lambda_P$, because $\cos(k_1 x)$ is almost a constant in the narrow region $\lambda' \equiv 1/\sqrt{\zeta q|\text{Re}(A_1)\cos(k_1 x_0)|}$, Eq. (28) can be approximated as

$$\lambda'^2 \partial_x^2 P^{s0} = \sin P^{s0}. \tag{29}$$

Equation (29) has the usual soliton solution $P^{s0} = 4\arctan\{\exp[(x-x_0)/\lambda']\}$. The total resultant P_l^s is $(2m$

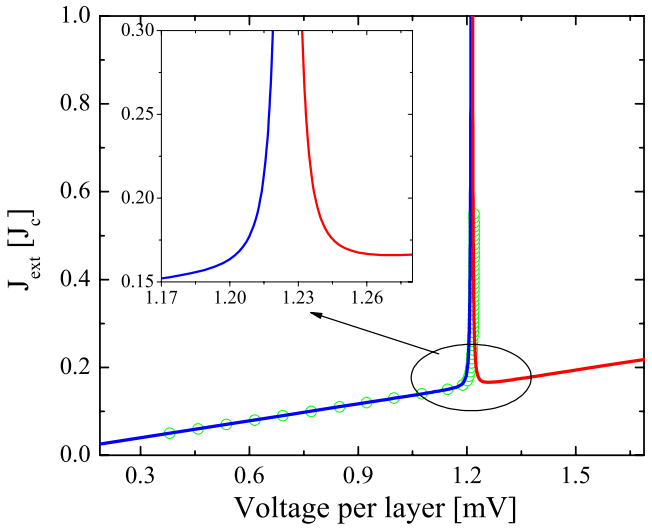

FIG. 3. (Color online) *IV* characteristics calculated by numerical simulations (symbols) and the linearized theory (lines). The inset is an enlarged view.

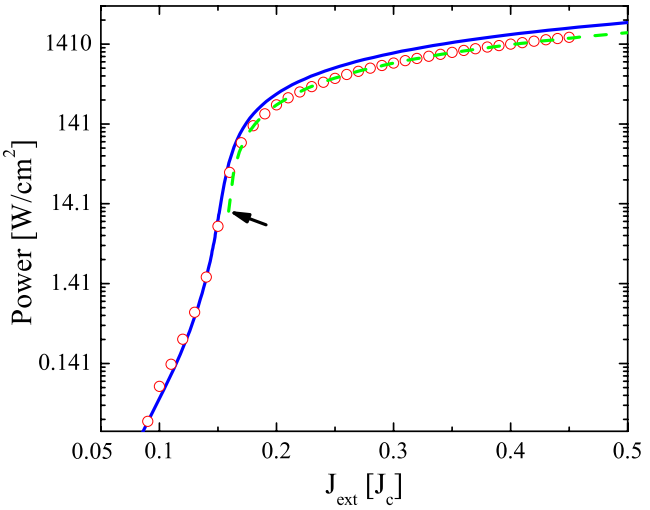

FIG. 4. (Color online) (a) Radiation power at the first current step obtained by simulations (symbol), the linear theory (solid line), and the power balance relation Eq. (33) (dashed line). The results are obtained with $C=0.000\,177$ and $R=707.1$. The arrow is the starting point of the first current step.

$+1)\pi$ phase kink at the center of junction and solitons with $\pm 2\pi$ phase variation away from the center of junction. The solitons with $\pm 2\pi$ phase variation do not contribute to F_1 as well as the net supercurrent, and therefore are omitted in the following discussions.

The *IV* characteristics shown in Fig. 3 is calculated from Eq. (26). One remarkable feature in the *IV* characteristics is the self-induced current step, i.e., *IV* branch with constant voltage. From Eq. (26), it is found that the *IV* characteristics for kink solutions with different m, e.g., the kink solutions in Figs. 2(c), 2(e), 2(g), and 2(i), is almost the same, because the kink renders itself approximately as a step function and the dc current contributed from the kink region of width λ_P is negligible. It should be noted that there exist two branches at the cavity resonance, and the right branch has a negative differential resistance.

The radiation power can be readily calculated from Eq. (16). With the linear approximation, the power is

$$S_r = \cos\,\theta |A_1 \omega|^2 / 2|Z|. \tag{30}$$

The dependence of S_r on θ and $|Z|$ is consistent with the results shown in Fig. 5 of Ref. 30. The results of S_r are displayed in Fig. 4. Similar to the *IV* characteristics, the radiation powers for the states with different phase-kink configurations are almost the same.

To check the applicability of the analytical treatment, we solve the equation of motion Eq. (11) by computer simulations.[30] The time step in all simulations is set to $\Delta t = 0.0018$ and the mesh size is set to $\Delta x = 0.002$. The accuracy is checked with smaller Δt and Δx. We use the periodic boundary condition along the z axis to minimize the surface effect, and attach an effective RC circuit to the junctions as the boundary condition along the x direction.[50,51] In this case, the impedance is $Z = R - i/C\omega$, where R is the resistance and C is the capacitance of the RC circuit. R and C are chosen to make sure that $|Z| \gg 1$.

The simulation results of the *IV* characteristics and radiation power are presented in Figs. 3 and 4. For the *IV* characteristics, there is good agreement between the theory and simulation, except that the theory is incapable of describing the height of the current step. For the radiation power, the linear theory is valid off or near resonance but fails inside the current steps. The failure of the analytical treatment is caused by the strong plasma oscillation and existence of harmonics in the current step.[30]

To derive a better estimate of the power radiation at the current steps, we resort to the power balance equation which is valid in the whole region of the *IV* characteristics. Taking the plasma solution Eq. (17) and substituting into the power balance equation Eq. (14), we obtain the *IV* characteristics in the presence of radiation

$$\omega J_{\text{ext}} = \beta\omega^2 + \frac{\beta}{4}\sum_{j=1}^{\infty}(j\omega A_j)^2 + \frac{\cos\,\theta}{L|Z|}\sum_{j=1}^{\infty}(j\omega A_j)^2. \tag{31}$$

In other words, the radiation power can be evaluated if we know the *IV* characteristics. Therefore it is useful to introduce an effective conductance β' defined as

$$J_{\text{ext}} = \beta'\omega = (\beta + \beta_d + \beta_r)\omega, \tag{32}$$

where $\beta_d \equiv \frac{\beta}{4}\Sigma_{j=1}^{\infty}(jA_j)^2$ is the conductance due to damping of plasma oscillation, $\beta_r \equiv \frac{\cos\,\theta}{L|Z|}\Sigma_{j=1}^{\infty}(jA_j)^2$ is the conductance due to radiation at both edges. From Eq. (31), we can calculate A_j from the *IV* characteristics. The radiation power at one edge then can be evaluated by

$$S_r = \beta_r\omega^2/2 = J_e\omega \Big/ \left(\frac{\beta|Z|}{2\,\cos\,\theta} + \frac{2}{L}\right), \tag{33}$$

where $J_e \equiv J_{\text{ext}} - \beta\omega$ is the excess current. From the foregoing analysis, if we can screen the radiation at one edge, the radiation at the other edge is enhanced. It should be remarked

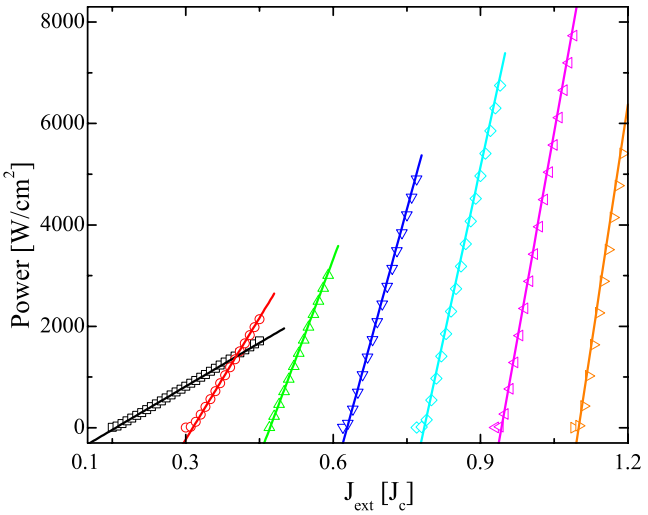

FIG. 5. (Color online) Radiation power on current steps. The symbols are from the simulations and the lines are given by Eq. (33). The results are obtained with $C=0.000\,177$ and $R=707.1$.

that not the whole energy pumped into plasma oscillation radiates into outside space. Most part of it is damped by dissipations inside the intrinsic Josephson junctions. The radiation power at current steps obtained by numerical simulations and power balance condition is depicted in Fig. 5. In contrast to the linear approximation, the estimated radiation power by Eq. (33) is consistent with simulations even inside the current steps where the amplitude of plasma oscillation is large and high harmonic components are present. The power increases linearly with the $J_{\rm ext}$ and the maximum power is as high as 8000 W/cm^2 from simulations (at the sixth cavity mode). The maximal total radiation power at the first cavity mode is about 10 mW if we use a mesa of similar dimension as the experiments,[27] which is capable of practical applications.

The cavity quality factor Q_c at the cavity resonance $\omega = k_1$ is given by

$$Q_c \equiv \omega \frac{\text{Energy Stored}}{\text{Power Loss}} = \frac{\omega}{\beta + 4\cos\theta/L|Z|}, \tag{34}$$

which has the order of magnitude of 100 for $\beta=0.02$ and $|Z| \gg 1$. The half-width of the radiation frequency spectrum $\Gamma = \omega/Q_c$ is about 10 GHz, so that the radiation is almost monochromatic. The efficiency defined as the ratio of the radiation power to the total power input is

$$Q_e = \frac{J_e}{J_{\rm ext}} \Big/ \left(\frac{\beta|Z|}{4\cos\theta} + \frac{1}{L} \right). \tag{35}$$

The efficiency Q_e at the current step corresponding to a lower cavity mode is larger than that of a higher mode because of the smaller Ohmic dissipations. Q_e at the top of the first current step in Fig. 5 is about 7.5%.

The distribution of the c-axis uniform electromagnetic (EM) wave along the x direction of the junctions, as well as the supercurrent, obtained from simulations at the bottom and top of the first current step are shown in Fig. 6. The supercurrent has the same period as P_l^s along the c axis, and we only visualize it at one layer. We divide the Josephson current into the symmetric part $J_{\rm sym}$ and antisymmetric part $J_{\rm asym}$ with respect to the center of junction, i.e., $\sin P_l(x) = J_{\rm asym}(x) + J_{\rm sym}(x)$. Off resonance, $J_{\rm sym}$ is zero except the center of junction, while $J_{\rm asym}$ oscillates from -1 to $+1$; the magnetic field is symmetric and electric field is antisymmetric with respect to the center of junction. However, at the top of the current step, the even part of Josephson current becomes more important, so the radiation is of dipole type. The corresponding distribution for EM wave is neither symmetric nor antisymmetric because the higher harmonics in Eq. (17) become important.

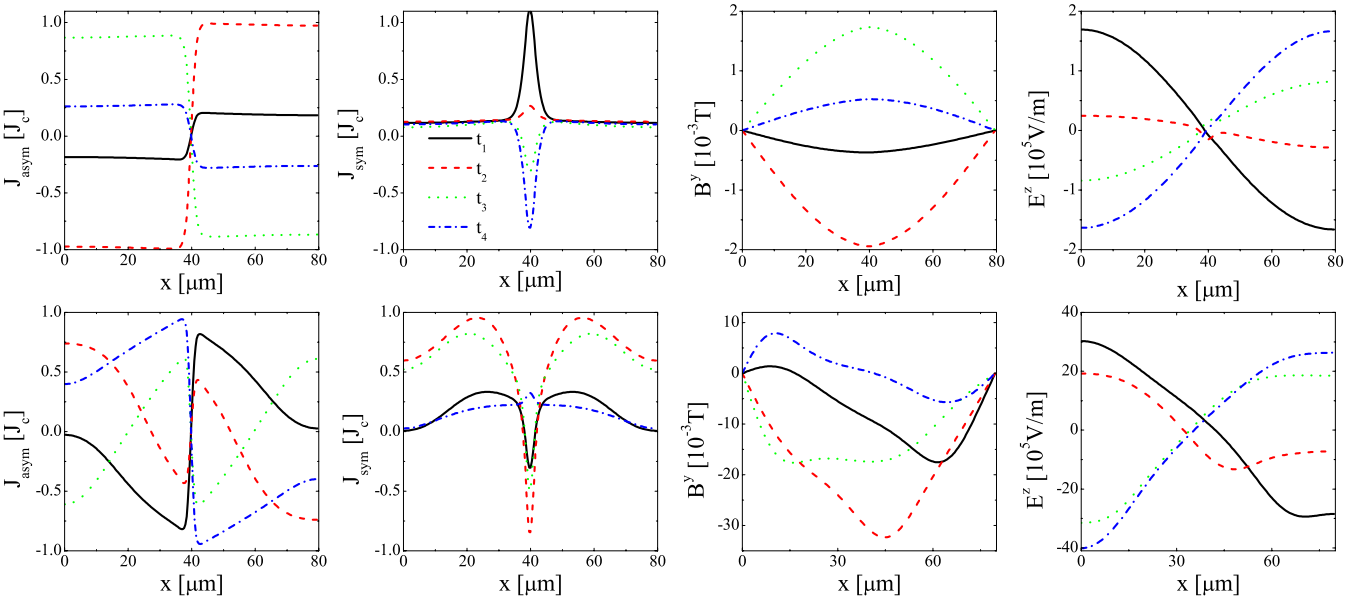

FIG. 6. (Color online) Configurations of $J_{\rm asym}$, $J_{\rm sym}$ and electromagnetic wave at successive time $t_1=0.06T_1$, $t_2=0.31T_1$, $t_3=0.83T_1$, and $t_4=0.94T_1$, where $T_1 \equiv 2\pi/k_1$ is the period of plasma oscillation at the first cavity mode. We have subtracted the static part of E^z. The top figures are taken at the bottom of the first current step while the bottom figures are at the top of the first current step in Fig. 3.

B. State without kink

Equation (27) also has trivial vacua solutions $P^{s0}=m\pi$. Without losing generality, we take $m=0$. From Eq. (25), we know that the transverse plasma cannot exist without a kink. Therefore the solution becomes

$$P_l = \omega t - iA_1 \exp(i\omega t), \tag{36}$$

which is nothing but the McCumber solution. Here only the fundamental mode is taken, which is sufficient because of the small plasma oscillation in this solution. Then Eq. (25) is reduced to

$$A_1 = 1/(\omega^2 - i\beta\omega), \tag{37}$$

and its corresponding IV characteristics without radiation is

$$J_{\text{ext}} = \beta\omega + \frac{\beta}{2(\omega^3 + \beta^2\omega)}. \tag{38}$$

The radiation power at one edge obtained with Eq. (16) is

$$S_r = \cos\theta/[2(\omega^2 + \beta^2)|Z|]. \tag{39}$$

From the power balance condition, the IV characteristics with radiation is given by

$$J_{\text{ext}}\omega = \beta\omega^2 + \frac{\beta}{2(\omega^2 + \beta^2)} + \frac{\cos\theta}{(\omega^2 + \beta^2)|Z|L}, \tag{40}$$

where the last term represents the correction due to radiation. The minimum value of J_{ext} in Eq. (40) is the retrapping current J_r, at which the input power becomes insufficient for the phase particle to travel across the damped tilted washboard potential. In the weak damping limit $\beta \ll 1$ as in the present system, J_r is

$$J_r = \frac{4}{3}\beta^{3/4}\left(\frac{3\cos\theta}{|Z|L} + \frac{3\beta}{2}\right)^{1/4}. \tag{41}$$

Its corresponding voltage is $\omega_r=(1.5+3\cos\theta/|Z|L\beta)^{1/4}>1$, which justifies the approximation made in Eqs. (36) and (37).

The IV characteristics calculated from the analytic formula and numerical simulations are presented in Fig. 7. Good agreement between the simulation and theory can be spotted. This further verifies the approximation of neglecting the effect of radiation on the phase dynamics in junctions when Z is large. The radiation power increases continuously with decreasing current and reaches the maximum at the retrapping point. The local minima in the curve are caused by the small spatial modulation of electromagnetic field, which changes with the voltage, similar to a cavity behavior. The frequency harmonics is indiscernible even at the maximum radiation because the plasma oscillation is weak. The distributions for P, B^y, and E^z obtained by numerical simulations with open boundary condition are displayed in Fig. 8, where there is a small phase gradient created by radiation which is hard to see in the present scale. The magnetic field is antisymmetric with respect to the center of the junction, while the electric field is almost uniform along the x direction, except the small modulation created by radiation.

The state without kink (McCumber state) is unstable in the certain region of IV curve. In a long Josephson junction,

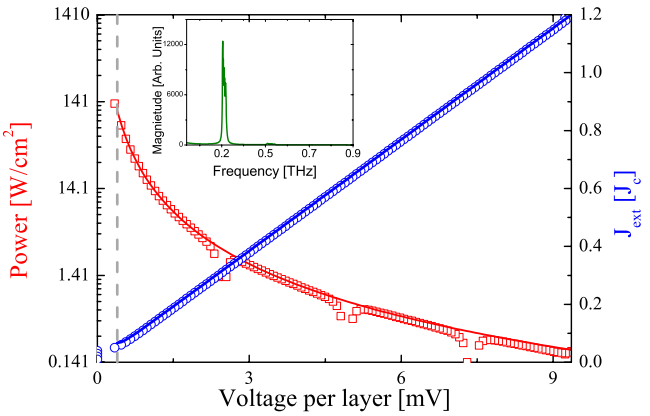

FIG. 7. (Color online) Radiation power from the state without kink and its corresponding IV characteristics. Symbols are for simulations and lines are for theory. The vertical dashed line is the retrapping point obtained from the theory. The inset is the frequency spectrum at the strongest radiation. The results are obtained with $C=0.716$ and $R=10.0$.

the system evolves into soliton states due to the parametric instability.[52] We have investigated the stability of the state without kink in a stack of intrinsic Josephson junctions. The system favors the state with kink due to the instability of the state without kink near the cavity resonance.

IV. ENERGETIC ANALYSIS

Similar to conventional laser systems, most part of the input power is stored and dissipated in the junctions and only a small portion radiates into space. Therefore it is worthy of looking at the energy oscillation inside the junctions. One might consider that the state with kink costs more energy than that without kink. To see whether the state with kink can be realized in reality, it is necessary to know the energy cost to construct the kink. In this section, we calculate the energy stored in the intrinsic Josephson junctions.

As can be read from Eq. (7), the system energy consists of the magnetic energy E_B, electric energy E_E, and Josephson coupling E_J,

$$E_B = \langle \partial_x \mathbf{P}^T \mathbf{M}^{-1} \partial_x \mathbf{P} \rangle_{xt}/2N,$$

$$E_E = \langle \partial_t \mathbf{P}^T \partial_t \mathbf{P} \rangle_{xt}/2N,$$

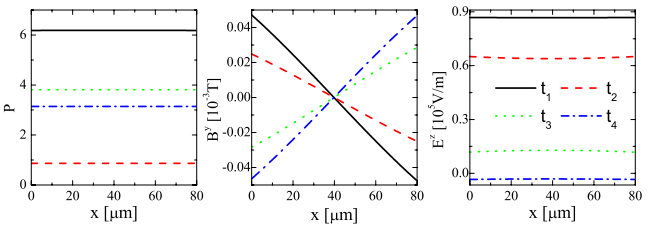

FIG. 8. (Color online) Configurations of phase P, magnetic field B^y, and electric field E^z at successive time $t_1=0.07T_r$, $t_2=0.17T_r$, $t_3=0.33T_r$, and $t_4=0.4T_r$, where T_r is the period at the retrapping point. The phase is normalized into $[0,2\pi]$ and we have subtracted the static part of E^z. The results are obtained by simulations with $C=0.716$ and $R=10.0$.

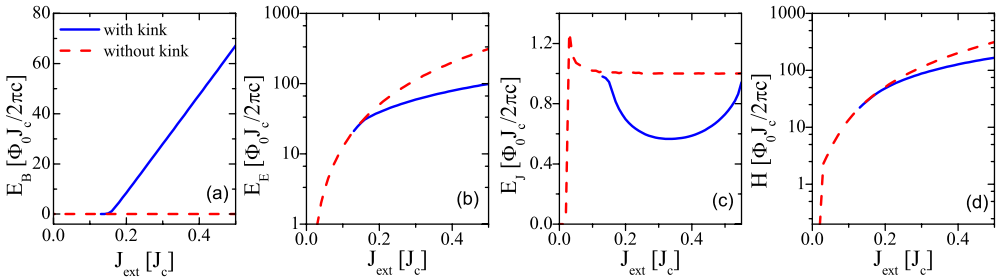

FIG. 9. (Color online) Energy per junction stored in a thick stack of intrinsic Josephson junctions in the state with and without kink, (a) magnetic, (b) electric, (c) Josephson, (d) total energy. The results are obtained without radiation, and the results for the state with kink are obtained in the first current step shown in Fig. 3. Because the energy for different kink configurations is same, only the energy for the kink configuration $\mathbf{P}^{sT}=[-\pi,+\pi,-\pi,+\pi]$ is shown in this figure.

$$E_J = \left\langle \sum_l (1-\cos P_l) \right\rangle_{xt} \Big/ N,$$

where the energy has been normalized by the number of layers N. In the state with kink, the magnetic energy has contribution from the static kink $E_{\mathrm{Bs}}=\langle \partial_x \mathbf{P}^{sT}\mathbf{M}^{-1}\partial_x \mathbf{P}^{s}\rangle_{xt}/2N$ and from the plasma oscillation $E_{\mathrm{Bp}}=\langle \partial_x \tilde{\mathbf{P}}^{T}\mathbf{M}^{-1}\partial_x \tilde{\mathbf{P}}\rangle_{xt}/2N$. Here we show that $E_{\mathrm{Bs}} \ll E_{\mathrm{Bp}}$. From Eq. (28), $\partial_x P_l^s$ has the order of magnitude $\sqrt{\zeta q|\mathrm{Re}(A_1)|}$ in the narrow region $1/\sqrt{\zeta q|\mathrm{Re}(A_1)|}$. Thus, the order of E_{Bs} is $\sqrt{|q\ \mathrm{Re}(A_1)|/\zeta} \ll 1$. On the other hand, E_{Bp} is proportional to $(A_1 k_1)^2$, which is of order of 10 with the parameters used in the present system. This also indicates that the magnetic energy for different kinks is roughly the same [thus we only show the magnetic energy for one kink configuration in Fig. 9(a)]. It is quite different from the usual solitons in a single Josephson junction.

With the linear expansion of Josephson current, similar to Eq. (26), the Josephson energy E_J in the state with kink can be obtained

$$E_J = 1 - \frac{(k_1^2-\omega^2)|F_1|^2/4}{(k_1^2-\omega^2)^2+\beta^2\omega^2}. \tag{42}$$

It first decreases and then increases inside the current step, while is close to unity off resonance. The calculation of the electric energy and total energy is straightforward. The results are shown in Figs. 9(b) and 9(d). The total energy for different kinks is approximately the same. Therefore the states with kink occupy finite volumes in the phase space with the same energy, which makes this state easily accessible.

In the state without kink, the magnetic energy is obviously zero. The Josephson coupling is

$$E_J = 1 + \frac{1}{2(\omega^2+\beta^2)}. \tag{43}$$

It decreases from its maximum at the retrapping point and saturates to unity at large currents, which is consistent with the results shown in Fig. 9(c). E_J in the region of $J_{\mathrm{ext}} < J_r$ is very close to 0, which cannot be described by Eq. (43) because the system is retrapped into superconducting state. The total energy is the same as that of state with kink in the linear Ohmic *IV* curve, while it is larger than that of state with kink in the current step.

The electric energies in Fig. 9 is much larger than other energy in the state without kink in a sharp contrast to cases at equilibrium, where different energy contributions are expected to be the same. The reason can be understood if we consider Eq. (11) as the equation of motion of phase particle in a titled washboard potential. In the presence of external current, the phase particle is accelerated and starts to run in the tilted washboard potential. In response to the modulated potential, small oscillations of phase particle are created in addition to the motion with a constant velocity. Meanwhile, the motion of phase particle causes dissipation. The steady state is reached when the input power and dissipation are balanced. On the other hand, the magnetic energy and Josephson coupling are solely contributed from the small oscillation of the phase particle. As the most part of input power converted into the motion with a constant velocity, the electric energy occupies the most part of energy stored in the system, as shown in Fig. 9. However, in the state with kink, as a significant portion of the input power is converted into plasma oscillation in the current steps, rather than to solely increase the velocity of the phase particle, the electric energy and magnetic energy become comparable to each other.

V. RADIATION PATTERN

In this section, we calculate the far-field radiation pattern for the mesa operated in the state with kink and without kink, which is important both for applications and for differentiating various states.

To calculate the radiation pattern, we resort to the Huygens principle in which the pattern is determined by the oscillation of the electromagnetic fields at the edges of samples, which can be casted into the edge magnetic current and electric current in the formula of equivalence principle.[53] Since there exists a significant impedance mismatch, the electric current produced by the oscillating magnetic field is much smaller than the magnetic current produced by the oscillating electric field, so we can neglect the contribution from the electric current. The equivalent magnetic current $\mathbf{M_e}$ in the dimensionless units is given by

$$\mathbf{M_e} = \mathbf{E_e} \times \mathbf{n}, \tag{44}$$

where $\mathbf{E_e}$ is the oscillating electric field at the edges of mesa and the vector $\mathbf{n}$ is normal to the edges. As we know that the

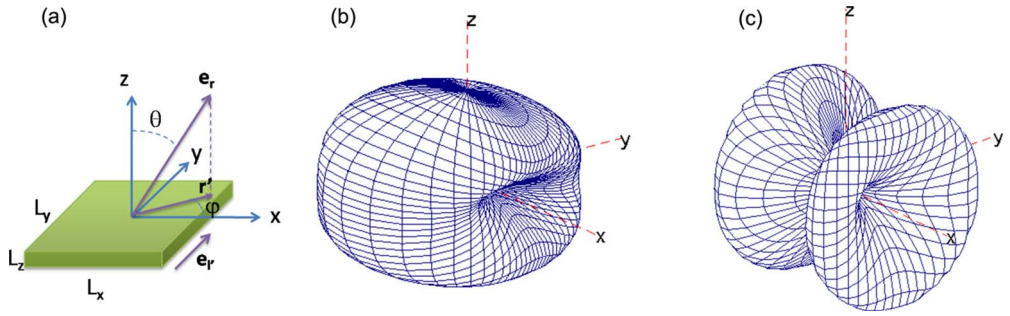

FIG. 10. (Color online) (a) Coordinate system for the calculation of radiation pattern from the mesa. (b) Radiation pattern of the mode (1,0). (c) Radiation pattern of the mode (1,1). Here $L_x=80$ μm, $L_y=300$ μm, and $L_z=1$ μm.

radiation pattern critically depends on the geometry of the source, we need to consider the three-dimensional (3D) system. The extension from previous analysis of two-dimensional (2D) system to 3D is given in Ref. 34. The coordinates for the 3D system are sketched in Fig. 10(a). We use the similar dimension as in the experiments,[27,29] i.e., $L_x=80$ μm, $L_y=300$ μm, and $L_z=1$ μm. Because $k_\omega L_z \ll 1$ with $k_\omega \equiv \omega/c$, the sources at different z coordinates do not interfere too much, and can be treated as uniform. In this case, the far-field Poynting vector in the dimensionless units is

$$\mathbf{S_r} = \frac{\omega^2 L_z^2}{32\pi^2 r^2 \varepsilon^{3/2}} |\mathbf{G}|^2 \mathbf{e_r}, \tag{45}$$

with

$$\mathbf{G} = \oint_{\text{edges}} M_e(r') \exp\left(-i\frac{\omega}{\sqrt{\varepsilon}}\mathbf{r}' \cdot \mathbf{e_r}\right)(\mathbf{e_r} \times \mathbf{e_{l'}})dl', \tag{46}$$

where the integral is taken over the perimeter of the crystal, $\mathbf{r}$ is the distance between the observer and the mesa and ε is the dielectric constant of vacuum normalized by ε_c. With the size we use, the interference is mainly contributed from the source along the y direction since L_y is comparable to the wavelength.

In the state with kink, the oscillation of the electric field in the frequency domain can be well described by

$$E_z = A_1 \omega \cos(n_x \pi/L_x)\cos(n_y \pi/L_y), \tag{47}$$

for the cavity mode (n_x, n_y) when the plasma oscillation is weak.[34] The radiation pattern from the mode (n_x, n_y) can be evaluated with Eq. (45) and is reported in Refs. 28 and 54. Inside the current step, the higher harmonics become important so numerical simulations are needed. We use computer simulations to calculate the oscillation of electric field at edges and then substitute the results into Eqs. (44) and (45) to obtain the radiation pattern. The results at current steps corresponding to the cavity modes (1,0) and (1,1) are shown in Figs. 10(b) and 10(c). For mode (1,0), the radiation power is maximal at the top of the mesa $\theta=0$, and it has a maximum at the middle of L_x while a minimum at the middle of L_y; for mode (1,1), the radiation power is minimal at the top of the mesa $\theta=0$, and at the middle of L_x and L_y.

In the state without kink, the oscillation of the electric field is homogenous in the xy plane, which corresponds to the (0,0) mode. The radiation pattern at the retrapping point is presented in Fig. 11. It has a minimum both at the top of the mesa and at the middle of L_y, and a maximum at the middle of L_x. The anisotropy of the pattern in the xy plane is due to the fact $L_y \gg L_x$.

VI. STATE WITH SOLITONS

To be comprehensive, we present here the results of numerical simulations on the state with solitons. It should be noted that in the present system, the length scale is λ_c rather than λ_J as in conventional Josephson junctions and in the presence of magnetic field. Therefore, to have solitons, the length of the junctions must be larger than λ_c. Because of repulsive interaction, it is believed to be hard to achieve in-phase motion of solitons in a stack of junctions, despite some simulations suggest that the solitons in high velocity have attractive interaction.[38,55] Here we investigate the radiation due to soliton motions in a single junction, which is equivalent to a stack of junctions if one realizes the in-phase motion of solitons in different junctions.

It is well known that periodic motions and reflections of solitons and antisolitons give birth to the zero-field steps at $V=2n\pi/L$, which corresponds to the even cavity modes,[56,57] with n the number of solitons. When a soliton hits the boundary, it emits an electromagnetic *pulse*.[58] Here we only investigate the radiation from zero-field steps and will not discuss the Cherenkov radiation.[59] We perform computer simulations

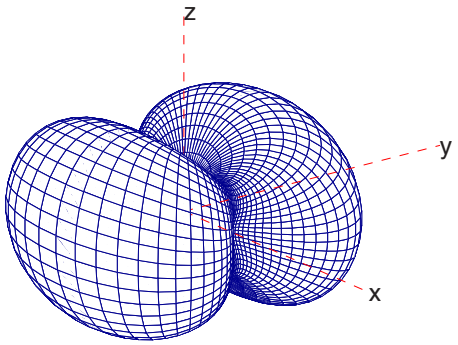

FIG. 11. (Color online) Radiation pattern of the state without kink biased at the retrapping point. Here $L_x=80$ μm, $L_y=300$ μm, and $L_z=1$ μm. The anisotropy of the pattern in the xy plane is due to the fact $L_y \gg L_x$.

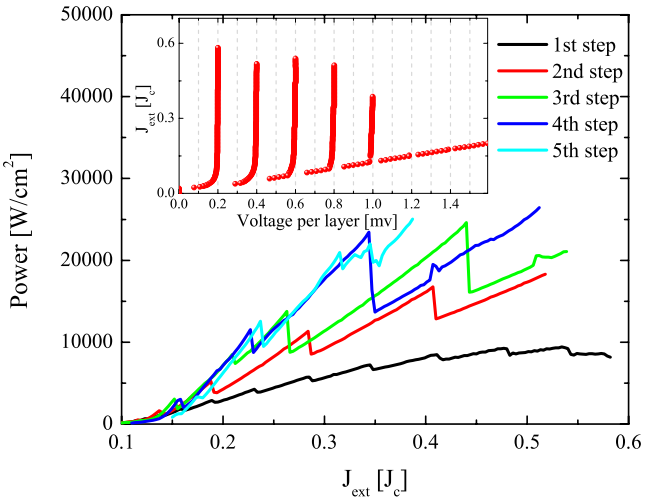

FIG. 12. (Color online) Radiation power from the zero-field steps caused by soliton motions. The inset is the *IV* characteristics. The vertical dashed lines are the assignment of cavity mode according to $k_n = n\pi/L$ with n being an integer and the ac Josephson relation. The results are obtained with $C=0.000\ 177$ and $R=707.1$.

to trace out all the zero-field steps. We use $L=5\lambda_c$ so that there exist five steps. The *IV* characteristics are shown in the inset of Fig. 12, where the zero-field steps occur at the voltage corresponding to the even cavity modes. The radiation power at each step is shown in Fig. 12, which is higher than that from the state with kink if one assumes in-phase motion of solitons. The discontinuous drops in the radiation power when ramping up the current are caused by the change in the wavelength of the Josephson plasma excited by the motion of solitons. The frequency spectrum at the first zero-field step is sketched in Fig. 13 and there are many frequency harmonics with the fundamental frequency not satisfying the ac Josephson relation. In the state with solitons, the radiated frequency depends on the configuration of solitons except the first zero-field step.[60] It is noticed that, as indicated in Fig. 13, the fundamental frequency and voltage at all the steps never satisfy the ac Josephson relation, contrasting with the state of kink revealed theoretically[30] and the experimental observations.[27,29]

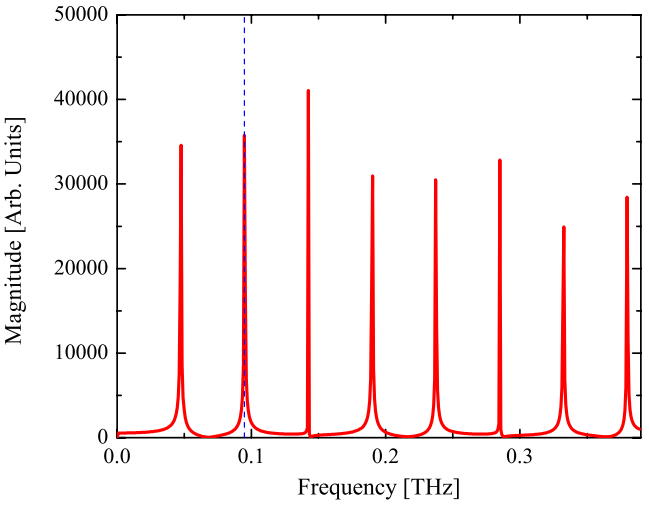

FIG. 13. (Color online) Frequency spectrum at the first zero-field step at $J_{ext}=0.57$. The vertical dashed line is the frequency given by the ac Josephson relation with voltage $V=2\pi/L$. The fundamental peak does not come to the dashed line means that the ac Josephson relation is broken. The results are obtained with $C=0.000\ 177$ and $R=707.1$.

VII. DISCUSSIONS AND CONCLUSIONS

In the present work, the phase dynamics and its electrodynamics in a thick stack of intrinsic Josephson junctions in the absence of external magnetic field are investigated both analytically and numerically. There is good consistency between the analytical theory and simulations.

In the state with phase kink, there are many current steps at both even and odd cavity modes. The phase kink plays a role of coupling the plasma to the cavity modes, as such the plasma oscillation is largely enhanced. The radiation power from the state with phase kink is ω^4 times larger than that without phase kink. The plasma oscillation is uniform through the c axis. Thus the far-field radiation power grows as N squared, the so-called super-radiation. At the bottom of the first current step, the magnetic field is symmetric with respect to the center of the junction. The antisymmetric component becomes more and more important when going into the current step. The states with different phase-kink configurations are degenerate in the sense that they have the same *IV* characteristics, power radiation, and energy stored in the system.

In the state without phase kink, the plasma oscillation does not couple to the cavity mode, and thus the radiation power is very small. The power increases with decreasing current and reaches the maximum at the retrapping point. The radiation occurs in a broad region of voltage. The frequency satisfies the ac Josephson relation, and high-frequency harmonics are almost invisible. The magnetic field is antisymmetric in this state. The far-field radiation pattern in this state is quite different from that in the state with phase kink, which is a clear fingerprint of the dynamic state realized by the system.

In the state with solitons, electromagnetic pulses are radiated from junctions when solitons hit the boundary. There are many frequency harmonics, but the fundamental frequency never satisfies the ac Josephson relation. It would be ideal for exciting strong terahertz wave with solitons because the power is about 25 000 W/cm^2, presuming one could realize the in-phase motion of solitons in a thick stack of long intrinsic Josephson junctions.

It is illuminating to discuss the dynamic state realized in the recent experiments for terahertz radiation[27,29] in light of the present theoretical analysis. Coherent radiations were detected in the resistive curve in Ref. 27 with the frequency corresponding to the first cavity mode. One order of the magnitude stronger radiations were observed in the region of voltage with anomalous *IV* characteristics in Ref. 29, and there are many frequency harmonics at a given voltage. In both experiments, the frequency obeys the ac Josephson effect and thus the state with traveling solitons can be ruled out. On the other hand, large cavity resonances cannot be

excited in the state without phase kink; furthermore, the radiation from the state without phase kink occurs weakly in a wide range of voltage. Therefore, it is unlikely relevant to the experimental observations. The state with phase kink, in contrast, seems to be consistent with the experiments so far. In this state, the plasma oscillation is uniform through the stack of Josephson junctions, it thus supports super-radiation as observed in the experiments. Moreover, the periodic arrangement of static kink along the stack direction allows to pump dc powers into large plasma oscillations, which yields self-induced current steps. It is noticed that, to obtain the overall shape of the *IV* curve, we need to take the heating effect into account. More works are needed to clarify the synchronization process.

It should be remarked that there are propagating waves besides the standing wave in Eq. (17) because of the radiation. The amplitude of the propagating waves has the order of magnitude of $1/|Z|$ and thus can be safely neglected as the first-step approximation, which is confirmed by the numerical simulations. The radiation has only some negligible effects on the dynamics inside the junctions, which permits us to calculate the radiation perturbatively. When the mismatch of impedance at the edges is reduced, e.g., the thickness of a stack of intrinsic Josephson junctions is comparable to λ_c, one has to consider the radiation and interference for the analysis of phase dynamics inside the junctions self-consistently.

The essential property of the stack of junctions for realization of the state with kink is the strong inductive coupling. As for other possible effects on the state with phase kink, we find in the simulations that this state is very stable against small magnetic fields, thermal fluctuations.[61] In Ref. 31, it is shown that the state with kink is stable against the modulation of critical current. Thus it is likely to be realized experimentally. The state with kink is promising for the application of terahertz radiation. It is also useful for terahertz detectors, amplifiers, and mixers.

ACKNOWLEDGMENT

The authors thank U. Welp, K. Kadowaki, M. Tachiki, L. Bulaevskii, A. Koshelev, N. Pederson, H. B. Wang, and T. Koyama for helpful discussions. They are also indebted to K. Kodowaki for showing them the experimental results prior to publication. Calculations were performed on SR11000 (HITACHI) in NIMS. This work was supported by WPI Initiative on Materials Nanoarchitronics, MEXT, Japan, CREST-JST, Japan, and partially by ITSNEM of CAS.

[1] B. Ferguson and X.-C. Zhang, Nature Mater. **1**, 26 (2002).
[2] M. Tonouchi, Nat. Photonics **1**, 97 (2007).
[3] I. K. Yanson, V. M. Svistunov, and I. M. Dmitrenko, Zh. Eksp. Teor. Fiz. **48**, 976 (1965).
[4] A. H. Dayem and C. C. Grimes, Appl. Phys. Lett. **9**, 47 (1966).
[5] J. E. Zimmerman, J. A. Cowen, and A. H. Silver, Appl. Phys. Lett. **9**, 353 (1966).
[6] N. F. Pedersen, O. H. Soerensen, J. Mygind, P. E. Lindelof, M. T. Levinsen, and T. D. Clark, Appl. Phys. Lett. **28**, 562 (1976).
[7] T. F. Finnegan and S. Wahlsten, Appl. Phys. Lett. **21**, 541 (1972).
[8] A. K. Jain, K. K. Likharev, J. E. Lukens, and J. E. Sauvageau, Phys. Rep. **109**, 309 (1984).
[9] M. Darula, T. Doderer, and S. Beuven, Supercond. Sci. Technol. **12**, R1 (1999).
[10] P. Barbara, A. B. Cawthorne, S. V. Shitov, and C. J. Lobb, Phys. Rev. Lett. **82**, 1963 (1999).
[11] R. Kleiner, F. Steinmeyer, G. Kunkel, and P. Müller, Phys. Rev. Lett. **68**, 2394 (1992).
[12] M. Tachiki, T. Koyama, and S. Takahashi, Phys. Rev. B **50**, 7065 (1994).
[13] T. Koyama and M. Tachiki, Solid State Commun. **96**, 367 (1995).
[14] M. Tachiki, M. Iizuka, K. Minami, S. Tejima, and H. Nakamura, Phys. Rev. B **71**, 134515 (2005).
[15] H. B. Wang, S. Urayama, S. M. Kim, S. Arisawa, T. Hatano, and B. Y. Zhu, Appl. Phys. Lett. **89**, 252506 (2006).
[16] L. N. Bulaevskii and A. E. Koshelev, J. Supercond. Novel Magn. **19**, 349 (2006).
[17] K. Kadowaki, I. Kakeya, T. Yamamoto, T. Yamazaki, M. Kohri, and Y. Kubo, Physica C **437-438**, 111 (2006).
[18] M.-H. Bae, H.-J. Lee, and J.-H. Choi, Phys. Rev. Lett. **98**, 027002 (2007).
[19] S. Z. Lin, X. Hu, and M. Tachiki, Phys. Rev. B **77**, 014507 (2008).
[20] S. E. Shafranjuk and M. Tachiki, Phys. Rev. B **59**, 14087 (1999).
[21] E. Kume, I. Iguchi, and H. Takahashi, Appl. Phys. Lett. **75**, 2809 (1999).
[22] K. Lee, W. Wang, I. Iguchi, M. Tachiki, K. Hirata, and T. Mochiku, Phys. Rev. B **61**, 3616 (2000).
[23] I. Iguchi, E. Kume, and H. Takahashi, Phys. Rev. B **62**, 5370 (2000).
[24] I. Iguchi, K. Lee, E. Kume, T. Ishibashi, and K. Sato, Phys. Rev. B **61**, 689 (2000).
[25] I. E. Batov, X. Y. Jin, S. V. Shitov, Y. Koval, P. Müller, and A. V. Ustinov, Appl. Phys. Lett. **88**, 262504 (2006).
[26] L. N. Bulaevskii and A. E. Koshelev, Phys. Rev. Lett. **99**, 057002 (2007).
[27] L. Ozyuzer, A. E. Koshelev, C. Kurter, N. Gopalsami, Q. Li, M. Tachiki, K. Kadowaki, T. Yamamoto, H. Minami, H. Yamaguchi, T. Tachiki, K. E. Gray, W.-K. Kwok, and U. Welp, Science **318**, 1291 (2007).
[28] A. E. Koshelev and L. N. Bulaevskii, Phys. Rev. B **77**, 014530 (2008).
[29] K. Kadowaki, H. Yamaguchi, K. Kawamata, T. Yamamoto, H. Minami, I. Kakeya, U. Welp, L. Ozyuzer, A. Koshelev, C. Kurter, K. E. Gray, and W.-K. Kwok, Physica C **468**, 634 (2008).
[30] S. Z. Lin and X. Hu, Phys. Rev. Lett. **100**, 247006 (2008).
[31] A. E. Koshelev, Phys. Rev. B **78**, 174509 (2008).
[32] H. Matsumoto, T. Koyama, and M. Machida, Physica C **468**, 654 (2008).

[33] M. Tachiki, Physica C **468**, 631 (2008).
[34] X. Hu and S. Z. Lin, Phys. Rev. B **78**, 134510 (2008).
[35] H. B. Wang, S. Guénon, J. Yuan, A. Iishi, S. Arisawa, T. Hatano, T. Yamashita, D. Koelle, and R. Kleiner, Phys. Rev. Lett. **102**, 017006 (2009).
[36] R. Kleiner, T. Gaber, and G. Hechtfischer, Phys. Rev. B **62**, 4086 (2000).
[37] S. Sakai, P. Bodin, and N. F. Pedersen, J. Appl. Phys. **73**, 2411 (1993).
[38] V. M. Krasnov and D. Winkler, Phys. Rev. B **56**, 9106 (1997).
[39] T. Koyama and M. Tachiki, Phys. Rev. B **54**, 16183 (1996).
[40] M. Machida, T. Koyama, and M. Tachiki, Phys. Rev. Lett. **83**, 4618 (1999).
[41] D. A. Ryndyk, Phys. Rev. Lett. **80**, 3376 (1998).
[42] S. Rother, Y. Koval, P. Müller, R. Kleiner, D. A. Ryndyk, J. Keller, and C. Helm, Phys. Rev. B **67**, 024510 (2003).
[43] L. N. Bulaevskii, D. Domínguez, M. P. Maley, A. R. Bishop, and B. I. Ivlev, Phys. Rev. B **53**, 14601 (1996).
[44] A. E. Koshelev and I. Aranson, Phys. Rev. B **64**, 174508 (2001).
[45] L. N. Bulaevskii and A. E. Koshelev, Phys. Rev. Lett. **97**, 267001 (2006).
[46] D. N. Langenberg, D. J. Scalapino, B. N. Taylor, and R. E. Eck, Phys. Rev. Lett. **15**, 294 (1965).
[47] R. Kleiner, Phys. Rev. B **50**, 6919 (1994).
[48] S. Sakai, A. V. Ustinov, H. Kohlstedt, A. Petraglia, and N. F. Pedersen, Phys. Rev. B **50**, 12905 (1994).
[49] J. Matisoo, Phys. Lett. **29A**, 473 (1969).
[50] N. Grønbech-Jensen, R. D. Parmentier, and N. F. Pedersen, Phys. Lett. A **142**, 427 (1989).
[51] C. Soriano, G. Costabile, and R. D. Parmentier, Supercond. Sci. Technol. **9**, 578 (1996).
[52] S. Pagano, M. P. Soerensen, R. D. Parmentier, P. L. Christiansen, O. Skovgaard, J. Mygind, N. F. Pedersen, and M. R. Samuelsen, Phys. Rev. B **33**, 174 (1986).
[53] W. L. Stutzman and G. A. Thiele, *Antenna Theory and Design* (Wiley, New York, 1998).
[54] M. Leone, IEEE Trans. Electromagn. Compat. **45**, 486 (2003).
[55] C. Gorria, P. L. Christiansen, Y. B. Gaididei, V. Muto, N. F. Pedersen, and M. P. Soerensen, Phys. Rev. B **68**, 035415 (2003).
[56] T. A. Fulton and R. C. Dynes, Solid State Commun. **12**, 57 (1973).
[57] A. V. Ustinov, Physica D **123**, 315 (1998).
[58] P. S. Lomdahl, O. H. Soerensen, and P. L. Christiansen, Phys. Rev. B **25**, 5737 (1982).
[59] G. Hechtfischer, R. Kleiner, A. V. Ustinov, and P. Müller, Phys. Rev. Lett. **79**, 1365 (1997).
[60] B. Dueholm, O. A. Levring, J. Mygind, N. F. Pedersen, O. H. Soerensen, and M. Cirillo, Phys. Rev. Lett. **46**, 1299 (1981).
[61] S. Z. Lin and X. Hu (unpublished).